A major purpose of the Technical Information Center is to provide the broadest dissemination possible of information contained in DOE's Research and Development Reports to business, industry, the academic community, and federal, state and local governments.

Although a small portion of this report is not reproducible, it is being made available to expedite the availability of information on the research discussed herein.

LA-UR -90-1113

LA-UR--90-1113

DE90 008967

TITLE: MODEL AND SIMULATIONS OF HYSTERESIS IN MAGNETIC CORES

AUTHOR(S): C. D. BOLEY, LLNL
M. L. HODGDON, M-6

SUBMITTED TO: 1989 INTERMAG CONFERENCE
WASHINGTON, DC, APRIL 1989

DISCLAIMER

Los Alamos

Los Alamos National Laboratory
Los Alamos, New Mexico 87545

MODEL AND SIMULATIONS OF HYSTERESIS IN MAGNETIC CORES

C. D. Boley
Lawrence Livermore National Laboratory, Livermore, CA 94550 USA

M. L. Hodgdon
Los Alamos National Laboratory, Los Alamos, NM 87545 USA

Using a theory of ferromagnetic hysteresis developed recently, we present simulations of the behavior of a ferrite core connected in series with an initially charged capacitor. Results are given for three materials and are shown to compare favorably with experiment.

Introduction

A classical problem in magnetic materials is the proper treatment of ferromagnetic hysteresis. Considerable effort has been given to cases in which the fields are confined to a limited region, such as the Rayleigh region, or along selected paths in the B-H plane. In this paper, we explore the implications of a more general hysteresis theory which has been developed recently [1,2]. In this theory, the permeability depends on B, H, and the rate of change of B according to

$$\mu(B, H, \dot{B}) = \{\alpha \operatorname{sign}(\dot{B}) [f(B) - H] + g(B, \dot{B})\}^{-1}, \tag{1}$$

where α is a constant and f and g are prescribed material functions. The theory applies throughout the B-H plane.

To test this theory, and to determine the values of some of its parameters, we apply the theory to the case of a toroidal ferrite core placed in a series circuit consisting of an initially charged capacitor, a switch, and the core itself, as shown in Fig. 1. After the switch is closed, the capacitor discharges through the circuit and the ferrite is driven into saturation. The fields then execute a series of loops in the B-H plane, with the loops decreasing in width. Simultaneously, the voltage exhibits damped oscillations of increasing period. We have developed a code in which the circuit voltages and currents, along with the magnetic variables, are obtained by the solution of a coupled nonlinear system consisting of the ferromagnetic hysteresis equations and the circuit equations.

Hysteresis Model

We use expressions for the material functions f and g discussed earlier [1,2], namely

$$f(B) = \begin{cases} A_1 \tan A_2 B, & \text{if } |B| \le B_{bp}; \\ A_1 \tan A_2 B_{bp} + (B - B_{bp})/\mu_i, & \text{if } B > B_{bp}; \\ -A_1 \tan A_2 B_{bp} + (B + B_{bp})/\mu_i, & \text{if } B < -B_{bp}, \end{cases} \tag{2}$$

$$g(B, \dot{B}) = \begin{cases} f'(B)\Big[1 - A_3\, c(\dot{B}) \exp(-\dfrac{A_4|B|}{B_d - |B|})\Big], & \text{if } |B| < B_d; \\ f'(B), & \text{otherwise}, \end{cases} \tag{3}$$

where μ_s is the permeability of the saturated material, and the constants A_1 and A_2 are related to the fields at closure, B_{cl} and H_{cl}, and the permeability, μ_{cl}, at the closure point via

$$A_1 = H_{cl}/\tan A_2 B_{cl}, \qquad A_2 = \sin(2A_2 B_{cl})/(2\mu_{cl} H_{cl}). \tag{4}$$

The "breakpoint" field B_{bp} is defined by

$$f'(B_{bp}) = 1/\mu_s, \quad \text{i.e.} \quad B_{bp} = \cos^{-1}(A_1 A_2 \mu_s)^{1/2}/A_2. \tag{5}$$

Values of the above parameters have been obtained from DC major loop data [1,2] and are given in Table 1.

Rate dependence enters into this theory through the dimensionless material function $c(\dot{B})$, which goes to unity as $\dot{B}$ approaches zero. Here it is taken to have the piecewise linear form

$$c(\dot{B}) = \begin{cases} 1 + c_1|\dot{B}|, & |\dot{B}| < \dot{B}_1; \\ 1 + c_1\dot{B}_1 + c_2(|\dot{B}| - \dot{B}_1), & \dot{B}_1 \le |\dot{B}| \le \dot{B}_2, \\ 1 + c_1\dot{B}_1 + c_2(\dot{B}_2 - \dot{B}_1), + c_3(|\dot{B}| - \dot{B}_2), & |\dot{B}| \ge \dot{B}_2, \end{cases} \tag{6}$$

where the quantities c_i and $\dot{B}_i$ are positive constants. This function can be expressed as the ratio of the coercive field, $H_c(\dot{B})$, to the dc coercive field, $H_c(0)$:

$$c(\dot{B}) = H_c(\dot{B})/H_c(0). \tag{7}$$

Alternately, as discussed in [2], it is the ratio of the energy loss w in a loop traversed at the rate $\dot{B}$ to the slow limit loss $w(0)$:

$$c(\dot{B}) = w(\dot{B})/w(0). \tag{8}$$

Values for the constants in Eq. (6) are obtained by using these expressions, energy loss measurements, and the experiments discussed here.

Core Model

We employ a one-dimensional model of the core in which the B and H fields are directed azimuthally and depend spatially only on r, the distance from the centerline. Thus Ampere's law (neglecting the displacement current) gives $H(r,t) = NI(t)/2\pi r$, where N is the number of windings. The constitutive relation implies that

$$\frac{\partial B(r,t)}{\partial t} = \mu(r,t)\frac{\partial H(r,t)}{\partial t}, \tag{9}$$

in which the permeability depends on (r,t) through its dependence on the local B and H fields. Applying Faraday's law, we see that the voltage across the core is related to the current according to $V_c(t) = L(t)dI(t)/dt$, where the time-dependent inductance is

$$\begin{aligned} L(t) &= \frac{N^2 h}{2\pi}\int_{r_{in}}^{r_{out}} \frac{\mu(r,t)}{r}\,dr \\ &\approx \frac{N^2 h}{2\pi}\sum_{k=1}^{N_s} \ln\left(\frac{r_{k+1}}{r_k}\right)\mu_k(t), \end{aligned} \tag{10}$$

in which h is the height of the core, and r_{in} and r_{out} are the inner radius and outer radius, respectively. For numerical purposes, we have divided the core into N_a concentric annuli, each having a permeability $\mu_k(t)$. In the simulations reported here, we represent the core by a single annulus, $N_a = 1$. The corrections associated with multiple annuli are small, typically of order 5-10%.

This information implies a set of ordinary differential equations for the quantities $V_c(t)$, $I(t)$, and the magnetic field $B(t)$. The functional dependence of the permeability renders this system highly nonlinear. The system is advanced in time via an ODE solver.

Results

We now turn to our specific results for the materials CN20 [3], C2025 [3], and VITROVAC [4]. The core sizes and circuit parameters [5] are listed in Table 2.

(a) CN20

The experimental voltage waveform, across the capacitor and a background resistance, is shown in Fig. 2. Hysteresis losses are prominent through the first several cycles, and rate dependence plays an important role. Values for the parameters that occur in Eq. (6) for $c(\dot{B})$ are obtained through the formulation of Eq. (7) and the approximation that during holdoff times (intervals when the voltage is at a plateau), the field in the core is nearly $H_c(\dot{B})$. Circuit analysis then yields

$$c(\dot{B}) = \frac{NC}{rH_c(0)}\frac{\Delta V}{\Delta t}, \tag{11}$$

where C is the capacitance, r is the average radius of the core, Δt is the holdoff time, and the voltage droop ΔV is the change in voltage during holdoff. Interpolation and smoothing give the parameter values listed in Table 3. As Fig. 2 shows, the calculated voltage waveform are in quite good agreement with experiment. The calculated hysteresis path is shown in Fig. 3. After six saturations, nearly all the initial energy is dissipated. In the higher energy loops, the permeability becomes negative near $B = 0$, while the narrower loops have positive permeabilities. The effects of rate dependence are revealed very dramatically when we compare this with the hysteresis path calculated for the case $c(\dot{B}) = 1$, shown in Fig. 4. We see that rate dependence has broadened the major loop by about a factor of 4, and that it yields a substantially greater energy loss, as reflected in the successively narrower minor loops. In Fig. 5 we show c as a function of time. This plot reflects the variations in V and hence those in $\dot{B}$.

Since the voltage is essentially constant between saturations, the magnetic field changes almost linearly with time in those intervals. Thus the holdoff times in Fig. 2 are given quite accurately by $\Delta t = NA\Delta B/\bar{V}$, in terms of the core area A, the flux swing $\Delta B = .94$ T, and the average plateau voltage $\bar{V}$.

(b) C2025

Two sets of circuit data are available for this material (runs B and C, Table 2). Since the first run exhibits greater core losses, we use it to determine, via Eq. (11), the rate dependent parameters which are listed in Table 3. As Fig. 6 indicates, the calculated voltage waveform can be made to agree well with the experimental waveform. To demonstrate the role of rate dependence, we show in the same figure the voltage which would result if $c(\dot{B})$ were set to unity for the entire run. Clearly the effect of values of c greater than unity is to lengthen the period and to increase the damping. The calculated hysteresis path is shown in Fig. 7.

Turning to the second set of circuit data, we compare in Fig. 8 the measured and calculated voltages. The calculated hysteresis path remains very close to the major loop and shows little rate dependence.

(c) VITROVAC

Figures 9 and 10 show the voltage traces and the hysteresis path for the amorphous magnetic material VITROVAC (run D). Values of the rate independent parameters are listed in Table 1. For this material, energy loss data for pulses of rates $\dot{B}$ ranging from 1 $T/\mu s$ to 100 $T/\mu s$ are available. Thus we can use both the method based on Eqs. (7) and (11) and the method based on Eq. (8) to calculate values for the rate dependent parameters. The results of the two methods were averaged and adjusted to give the parameter values listed in Table 3. Since the pulsed losses are almost constant for $\dot{B}$ less than 0.6 $T/\mu s$ and increase rapidly for greater values of $\dot{B}$, c remains fixed at unity for $\dot{B} < 0.6\ T/\mu s$.

Because the energy loss method is independent of the circuit parameters, it is preferable to the method described by Eqs. (7) and (11). One should note, though, that loss data reported at constant frequency, especially that for the Rayleigh region, cannot be applied here, since the present experiments are not characterized by a single frequency.

Conclusions

We have presented simulations of hysteresis experienced by a ferromagnetic core as it dissipates energy in an RLC circuit. Our calculations utilize the Hodgdon theory of ferromagnetic hysteresis, along with a model of the core geometry. The theory allows for both rate independent and rate dependent effects, with the latter often having a marked influence on the hysteresis. The hysteresis theory has a number of parameters, some of which are obtained from major loop data [1,2] and the others of which are deduced from circuit data.

Specific results have been obtained for three ferrites — CN20, C2025, and VITROVAC. For each of these, we have shown that the predicted voltage waveform can be brought into agreement with experiment. A viable theory should, of course, continue to agree with experiment when the circuit parameters are changed. We have verified this, to the extent that data are available, for C2025. As more data become available, we will be able to improve the precision of the model and to extend it to other materials.

Acknowledgments

We would like to thank W. A. Molander and B. E. Warner for stimulating discussions. We are also grateful to E. G. Cook for providing the experimental data. This work was performed under the auspices of the U. S. Department of

Energy by Lawrence Livermore National Laboratory under contract No. W-7405-Eng-48.

References

[1] M. L. Hodgdon, Applications of a Theory of Ferromagnetic Hysteresis, *IEEE Trans.* **MAG-24**, No. 1, 1988, pp. 218–221.

[2] M. L. Hodgdon, Mathematical Theory and Calculations of Magnetic Hysteresis Curves, *4th Joint MMM-Intermag Conference*, Vancouver, B.C., 1988.

[3] CN20 and C2025 are manufactured by Ceramic Magnetics, Fairfield, NJ.

[4] VITROVAC is manufactured by Vacuumschmelze GMBH, Hanau, DFR.

[5] The data were provided by E. G. Cook (private communication).

Table 1. DC material parameters. All quantities are in MKS units.

Material	B_{cl}	B_{bp}	H_{cl}	μ_s/μ_0	α	A_1	A_2	A_3	A_4
CN20	.4	.4103	397.9	2.	10.	21.19	3.794	-4.489	.3046
C2025	.4	.4181	1194.	2.	10.	119.7	3.677	-1.863	.2005
VITROVAC	.6	.6033	3.56	4.	2.5	.03299	2.603	-22.02	.2777

Table 2. Circuit parameters in individual runs. For the cores made of CN20 and C2025, the inner radius was 1 in, the outer radius was 2 in, and the height was 1 in. For the VITROVAC core, these dimensions were 1.55 in, 3.1 in, and .4 in, respectively. Since this core had a packing factor of .8, the radial width was shrunk such that the area was decreased by 20%.

Run	Material	V_0 (kV)	C (nF)	N_{turns}
A	CN20	6.08	8.10	4
B	C2025	5.98	8.10	4
C	C2025	5.77	18.9	9
D	VITROVAC	7.06	8.10	4

Table 3. Rate dependent material parameters (all in MKS units).

Material	$\dot{B}_1$	$\dot{B}_2$	c_1	c_2	c_3
CN20	7.5×10^5	∞	13.3×10^{-7}	8.0×10^{-7}	-
C2025	1.0×10^3	∞	2.0×10^{-4}	1.05×10^{-7}	-
VITROVAC	6.0×10^5	9.0×10^5	0.	1.0×10^{-3}	$.20 \times 10^{-3}$

FIGURE CAPTIONS

Fig. 1. Circuit employed in these simulations. The capacitor is initially charged, and the switch closes at $t = 0$. The quantities $R_1 = .1$ ohm and $R_2 = .1$ ohm are estimated background resistances associated with the windings and the capacitor, respectively. The results are insensitive to the precise values of these resistances.

Fig. 2. Calculated and observed voltages for CN20, run A, as a function of time. The voltage is across the capacitor and R_2. The solid line denotes the simulation, while the dotted line denotes the experiment. Because the location of $t = 0$ is experimentally uncertain, and also because the initial state of the core is unknown, we have shifted the experimental waveform such that the times of the first saturation agree.

Fig. 3. Calculated hysteresis path for CN20, run A, with the order of traversal as indicated.

Fig. 4. Calculated hysteresis path for CN20, run A, with rate dependence suppressed.

Fig. 5. Dynamic behavior of the rate dependent function c in the calculations for run A.

Fig. 6. Calculated and experimental voltage waveforms for C2025, run B. The same comment as in Fig. 2 applies. Also shown is the calculated voltage waveform with rate dependence ignored.

Fig. 7. Calculated hysteresis path for C2025, run B.

Fig. 8. Calculated and observed voltages for C2025, run C.

Fig. 9. Calculated and observed voltages for VITROVAC, run D.

Fig. 10. Calculated hysteresis path for VITROVAC, run D.

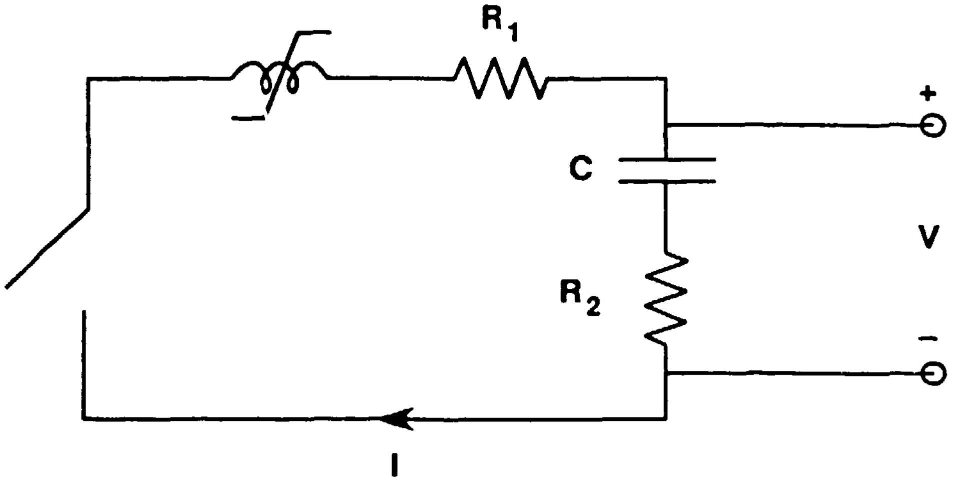

c.1.2.0169.0196

Fig. 1

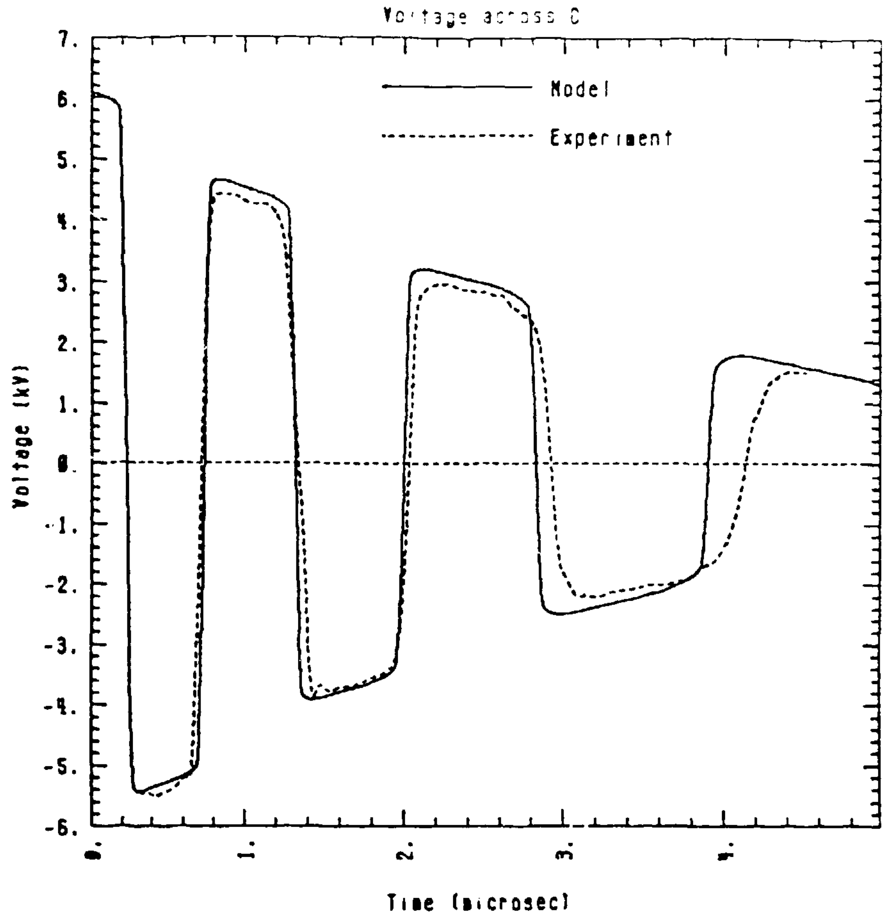
Voltage across C
Model
Experiment
Voltage (kV)
Time (microsec)
7.
6.
5.
4.
3.
2.
1.
0.
-1.
-2.
-3.
-4.
-5.
-6.
0.
1.
2.
3.
4.

Fig. 2

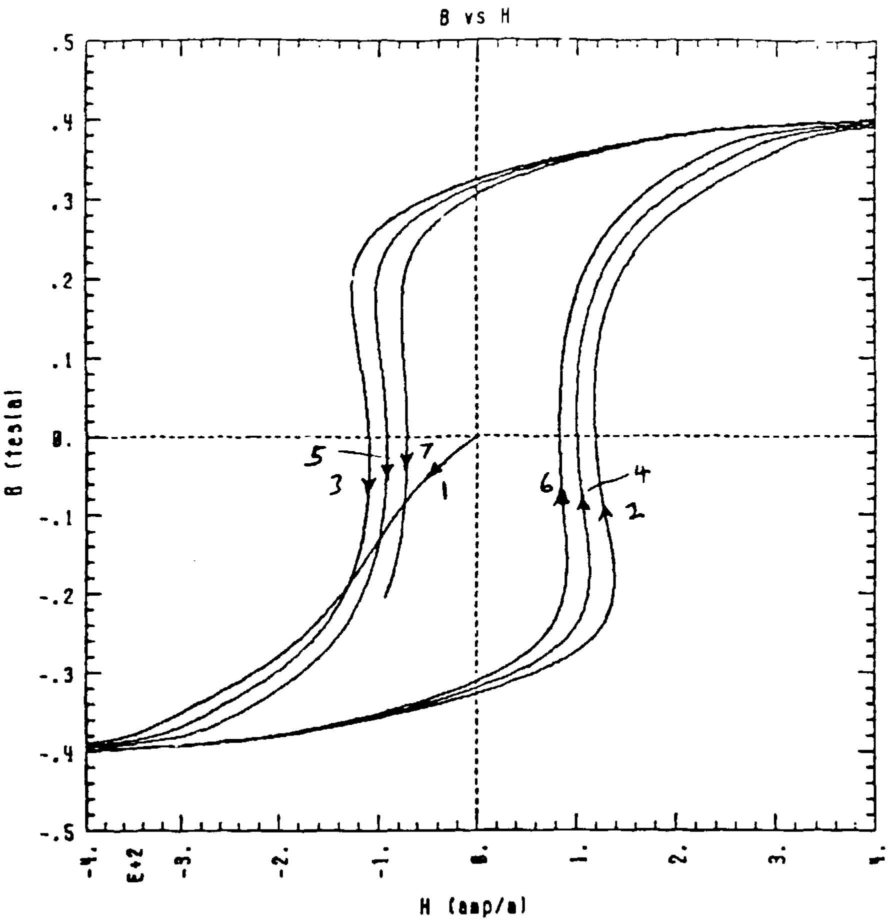

Fig. 3

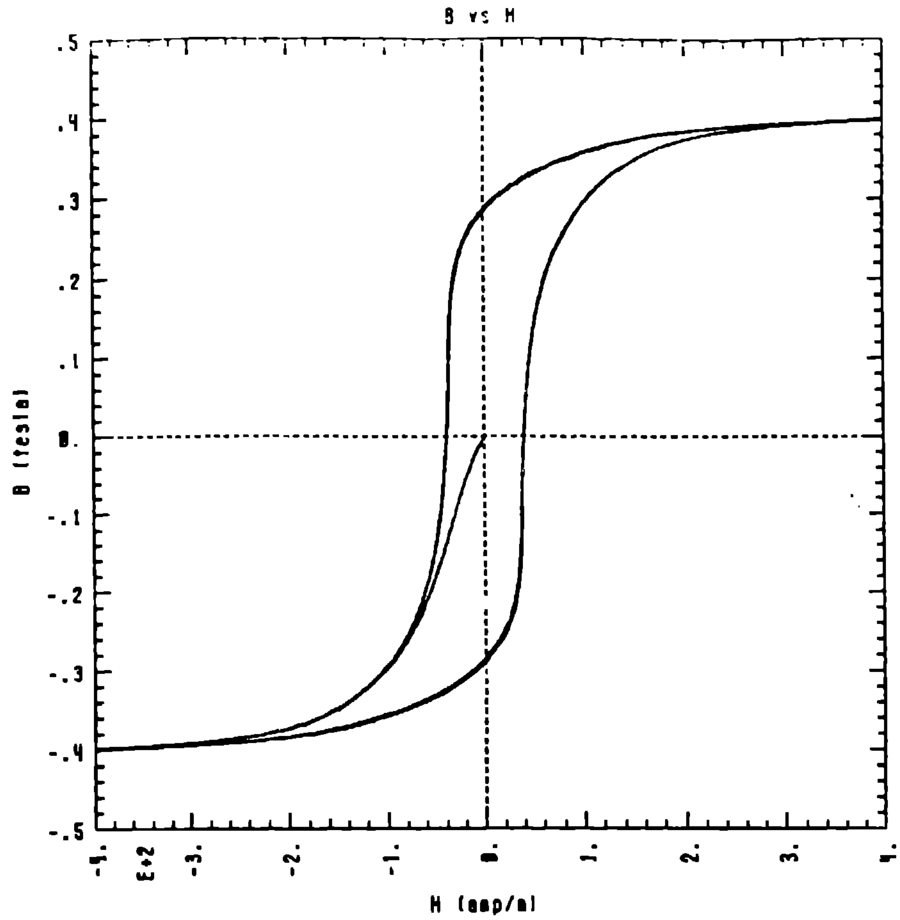

Fig. 4

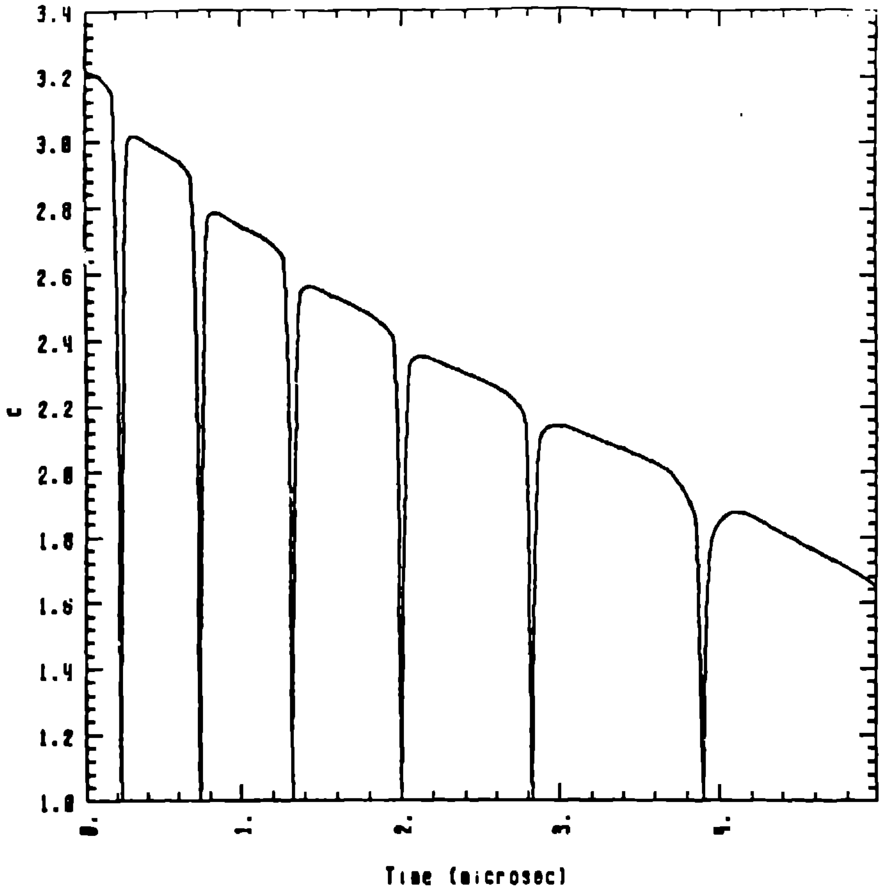

Fig. 5

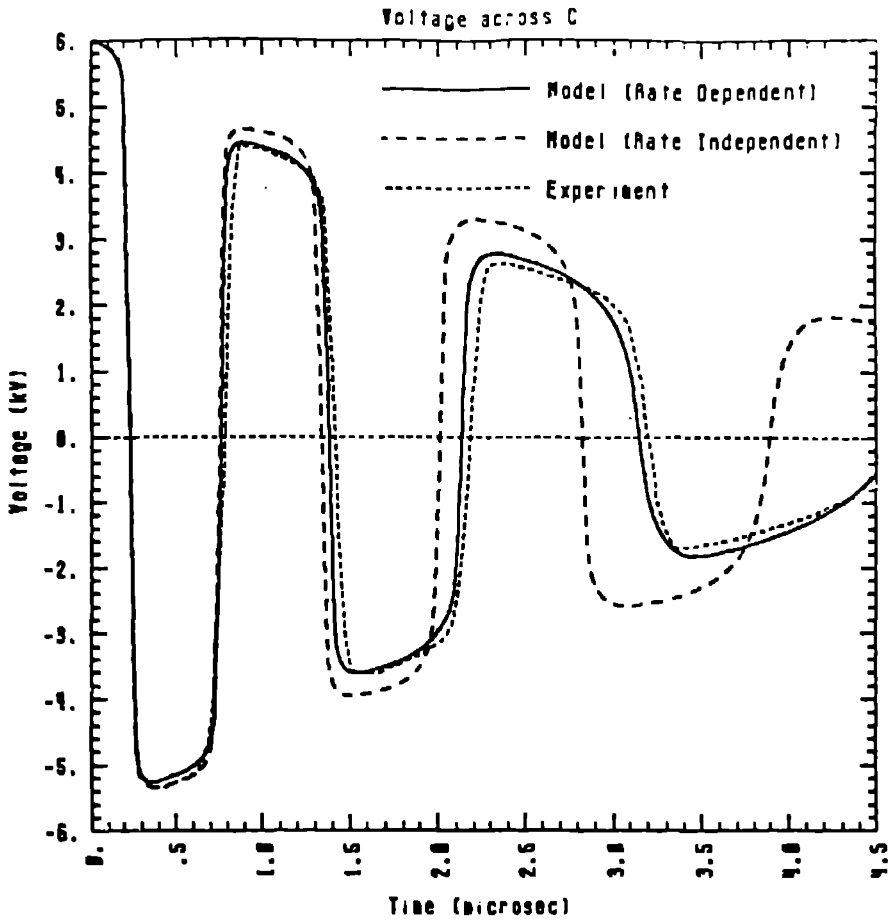
Voltage across C
Model (Rate Dependent)
Model (Rate Independent)
Experiment
Voltage (kV)
Time (microsec)

Fig. 6

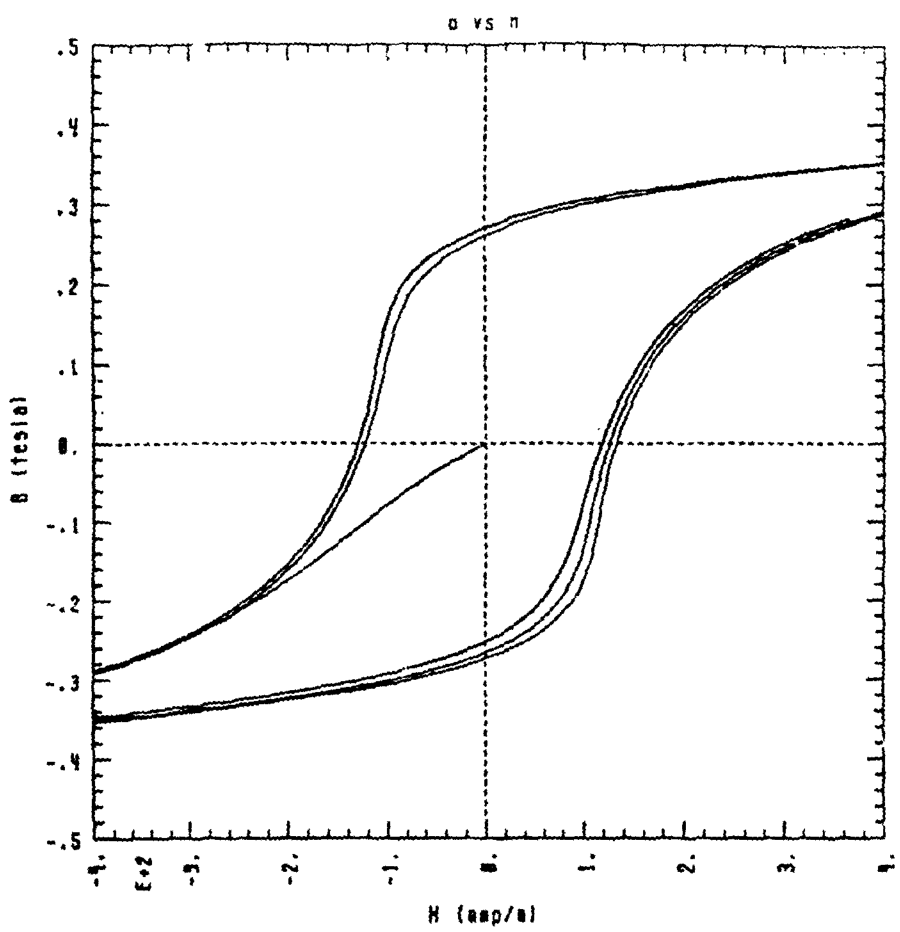

Fig. 7

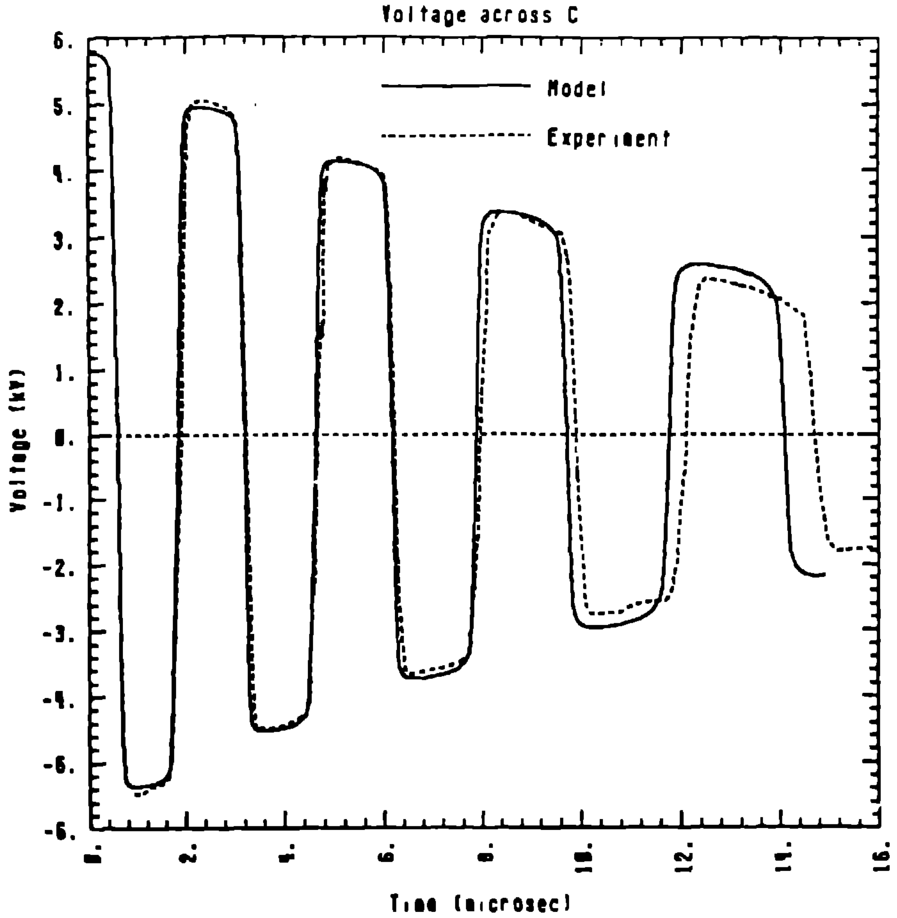
Voltage across C
Model
Experiment
Voltage (kV)
Time (microsec)
6.
5.
4.
3.
2.
1.
0.
-1.
-2.
-3.
-4.
-5.
-6.
0.
2.
4.
6.
8.
10.
12.
14.
16.

Fig. 8

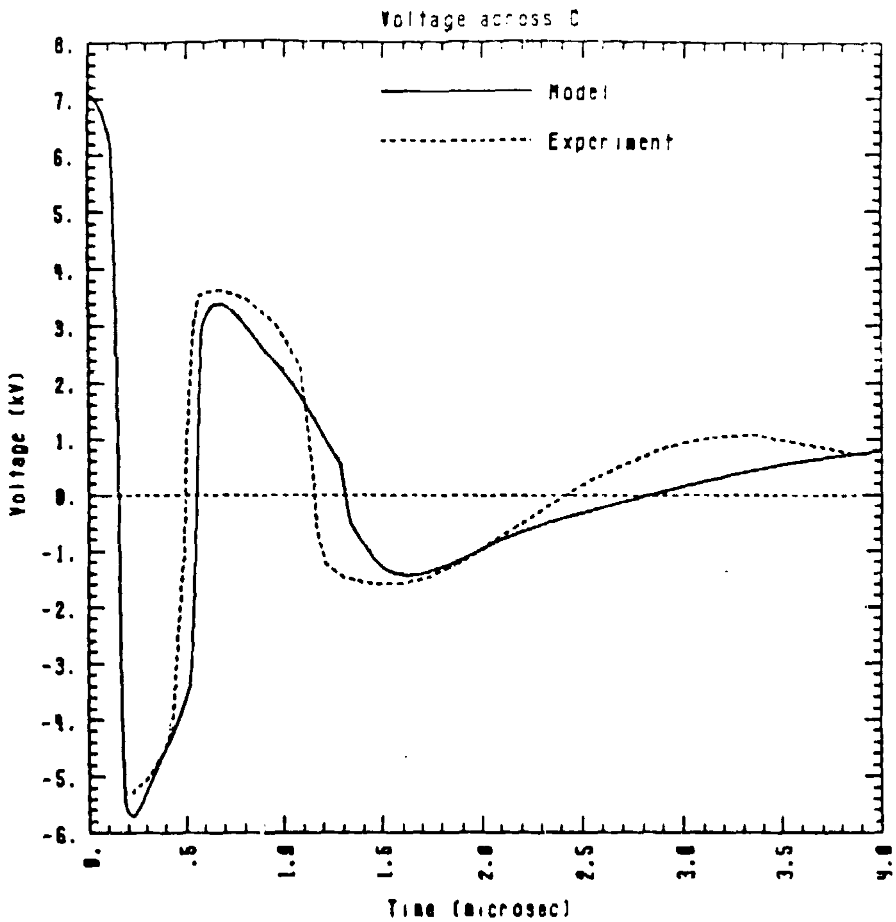

Voltage across C
Model
Experiment
Voltage (kV)
Time (microsec)

Fig. 9

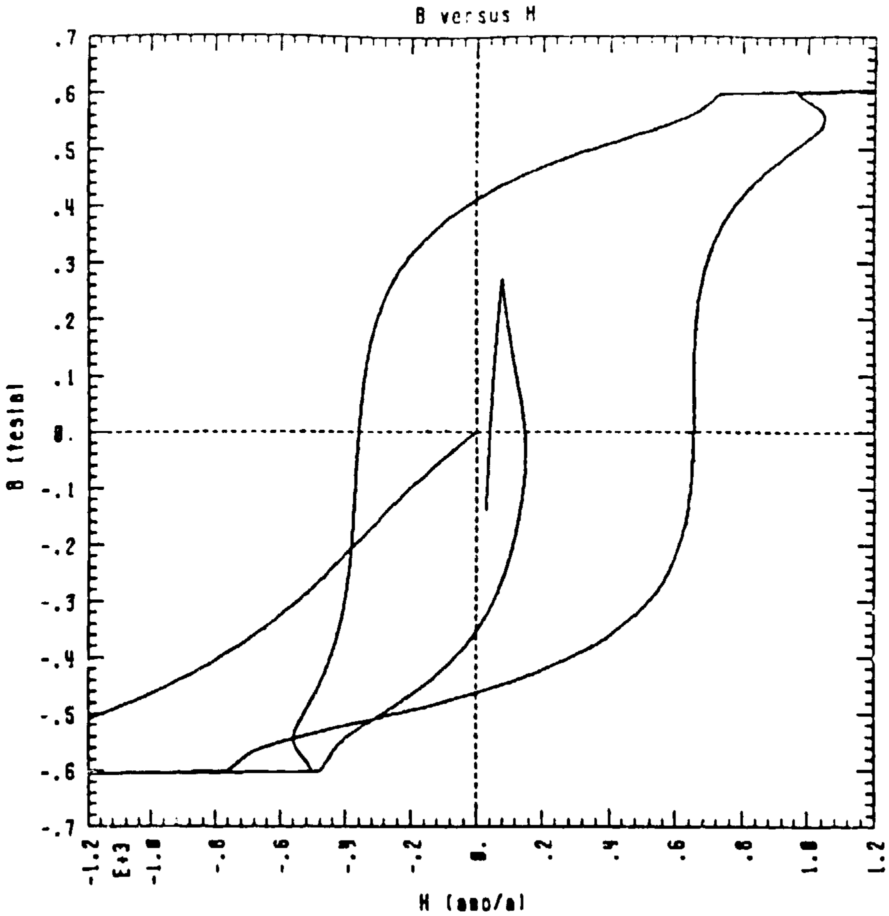
B versus H
B (tesla)
H (amp/m)
E+3
.7
.6
.5
.4
.3
.2
.1
0.
-.1
-.2
-.3
-.4
-.5
-.6
-.7
-1.2
-1.0
-.8
-.6
-.4
-.2
0.
.2
.4
.6
.8
1.0
1.2

Fig. 10